

# Design optimization and trajectory planning of a strawberry harvesting manipulator

Inas Saoud<sup>1</sup>, Hatim Idriss Jaafari<sup>1</sup>, Asaad Chahboun<sup>1</sup>, Naoufal Raissouni<sup>2</sup>, Nizar Ben Achhab<sup>1</sup>,  
Abdelilah Azyat<sup>1</sup>

<sup>1</sup>Mathematics and Intelligent Systems Research Team, National School of Applied Sciences-Tangier, Abdelmalek Essaadi University, Tangier, Morocco

<sup>2</sup>National School of Applied Sciences-Tetuan, Abdelmalek Essaadi University, Tetuan, Morocco

## Article Info

### Article history:

Received Nov 29, 2023

Revised Apr 18, 2024

Accepted May 17, 2024

### Keywords:

4-degree-of-freedom  
Denavit-Hartenberg method  
GlobalSearch algorithm  
Harvesting manipulator  
Mathematical modeling  
Modified sine jerk profile  
Workspace model method

## ABSTRACT

This paper presents a systematic approach to optimizing the structural parameters of a 4-degree-of-freedom (DoF) strawberry harvesting manipulator to minimize its workspace. Unlike previous research that primarily concentrated on the spatial needs related to fruit distribution areas, this work addresses the spatial dynamics of different stages of the fruit-picking process. This is achieved by combining the workspace model method, mathematical modeling, and the GlobalSearch algorithm in the optimization process. A comprehensive verification was conducted using the Denavit-Hartenberg method to simulate the workspace of the optimal manipulator structure. This ensured that the manipulator effectively covered the entire harvesting space. The research design involves exploring an optimal trajectory planning method by adopting a modified sine jerk profile that minimizes overall trajectory duration while maintaining good smoothness. The effectiveness of this method is demonstrated through a simulation of the trajectory of the four joints to drive the end effector from the initial position to the position of the strawberry. This approach yields execution times up to 27% shorter than in previous studies. The proposed method is useful for optimizing the physical and trajectory design of the harvesting manipulator that operates in confined and restricted environments to enhance efficiency, adaptability, and safety in harvesting operations.

*This is an open access article under the [CC BY-SA](#) license.*



## Corresponding Author:

Inas Saoud

Mathematics and Intelligent Systems Research Team, National School of Applied Sciences-Tangier

Abdelmalek Essaadi University

Tangier, Morocco

Email: inas.saoud@etu.uae.ac.ma

## 1. INTRODUCTION

Research has shown great interest in the development and implementation of harvesting robots. Most studies have focused on the identification and positioning of mature crops [1]–[3] and automatic navigation systems [4]–[6], while the design of the robot body is less affected. The manipulator is one of the main components of the harvesting robot; it must detach the fruit from the plant without damaging either the fruit or the plant. It's common to use industrial robotic arms that perform multiple tasks [7]. For example, Xiong *et al.* [8] used a robust Mitsubishi (RV-2AJ, Japan) industrial manipulator to harvest the strawberries. But its high price makes it inappropriate for use in agricultural fields. In addition, the small environment of tabletop cultivation restricted the robot adaptation, with a harvest success rate of 50% [9]. Industrial manipulators are generally very large, expensive, and complex to control [10], [11]. The development of a

well-designed strawberry harvesting robot that adapts to the narrow operating space of tabletop cultivation and meets the requirements of selective harvesting significantly enhances picking success. The performance of the manipulator is affected by the size of its parameters [12]. So the optimization of the manipulator's structural parameters is a prerequisite for its design in terms of performance indexes, which include accuracy, workspace, and energy consumption [13].

Sun *et al.* [14] optimized the structure parameters of a remote center-of-motion (RCM) mechanism by analyzing the kinematic performance and reachable space of the mechanism and then selecting the optimal mechanism parameters using the particle swarm optimization (PSO) algorithm. Xiong *et al.* [13] aimed to minimize the invalid workspace and achieve a compact structure by optimizing the structural parameters of the dual-apple-picking manipulator. First, they analyzed the relationship between the configuration parameters of the dual manipulator and its workspace. Then, they used the non-dominated sorting genetic algorithm II (NSGA-II) and the CRITIC-TOPSIS method to find the best solution. Zhang *et al.* [15] selected the workspace model method to optimize the structure parameters of tomato-picking manipulators. The optimization toolbox of MATLAB was used to generate the optimal solution. Zhu *et al.* [16] proposed a combined index that considers the area of the actual workspace and energy consumption to optimize the structure parameters of the hexapod walking robot leg. The combined index was minimized using the genetic algorithm.

Positioning accuracy and workspace minimization are important indexes for harvesting fragile fruit in a confined environment. However, combining various performance criteria in the optimization model necessitates a multi-stage process and extensive computational resources and time for achieving optimal results. This complexity may limit practical application, particularly as the complexity of the manipulator system rises, leading to increased computational and time requirements. The optimization of the manipulator's structural parameters to minimize its workspace is crucial, particularly in environments with limited space, such as between tabletop cultivation rows. This optimization is essential for enhancing efficiency and safety. Furthermore, improvements in the speed and accuracy of the manipulator's motion can be achieved through trajectory planning control.

The above studies adopted two methods to optimize the robot's workspace, which are the parameter analysis method [14] and the workspace model method [15]–[17]. The parameter analysis method examines individual parameters independently, neglecting their interdependencies and potentially ignoring constraints crucial for optimization. In contrast, the workspace model method globally models the robot's workspace, taking into account the interactions between parameters to determine the manipulator's workspace more efficiently. From the discussions, we begin by utilizing the workspace model method to define the spatial requirements for the harvesting task and analyze the manipulator's workspace configuration. This involves identifying the space needed for harvesting and ensuring it is enclosed within the manipulator's workspace. Using the information gathered from the workspace model method, we construct a mathematical model of the manipulator's workspace. This model incorporates structural parameters (link lengths and joint angles) and defines the workspace area and boundary constraints mathematically. This process facilitates the formulation of optimization objectives and constraints. Subsequently, the GlobalSearch algorithm is deployed to search for the optimal structural parameters that minimize the workspace area.

Various trajectory-planning approaches have been employed in harvesting manipulators. These approaches focus on smoothing the trajectory to minimize jerky movements and improve positional accuracy. Zhang *et al.* [15] used the cycloid trajectory method to generate joint movements of the tomato harvesting manipulator. This trajectory method improved the smoothness of the robot's motion by ensuring the continuity of the acceleration profile. Wu *et al.* [18] adopted fifth-order polynomial interpolation to generate the trajectory in the joint space of the picking manipulator. Cao *et al.* [19] selected quintic B-spline trajectory planning to obtain a smooth path for the 6-degree-of-freedom (DoF) series manipulator. Even though the cycloid and fifth-order polynomial trajectories ensure the continuity of the acceleration profile, higher levels of continuity are recommended for the harvesting manipulator as this task requires high precision. According to the study above, B-spline trajectory planning improves the continuity of the trajectory up to the jerk level, but it may impose heavy computation loads and require more travel time. Considering the earlier discussion, this work implements a trigonometric S-curve trajectory with the modified sine jerk model. This new trajectory planning method, which has not yet been used by the picking manipulators, enables a compromise to be found between smoothness, speed, and computational complexity.

## 2. METHOD

### 2.1. The configuration of the picking manipulator

The strawberries are cultivated in parallel rows on a tabletop. The fruits grow on both sides of the table, as shown in Figure 1. The platform moves along the centerline of the aisle between the plant rows and stops at the picking position to drive the manipulator to harvest the ripe crops one by one. The fruits are well

exposed, allowing a visual sensor to detect and locate them and a manipulator to access and detach them. Therefore, a small, lightweight, and compact four-DoF arm robot can complete the harvesting task between parallel rows because it occupies less space with a maximum workspace envelope [20]–[22].

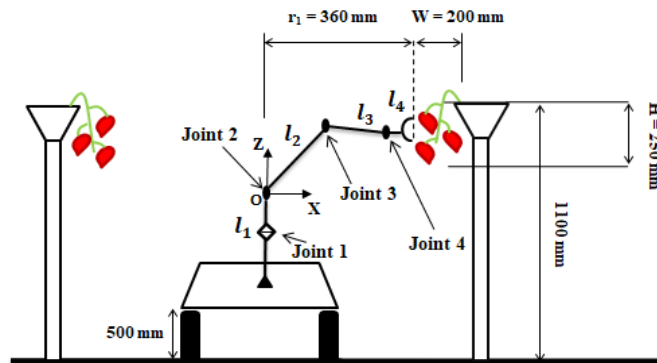


Figure 1. The structure of the agriculture robot and the strawberry distribution

$l_1$ ,  $l_2$ ,  $l_3$ , and  $l_4$  represent the lengths of the first link vertical to the base, upper arm, lower arm, and end-effector, as depicted in Figure 1. The  $[\theta_{1min}, \theta_{1max}]$ ,  $[\theta_{2min}, \theta_{2max}]$ ,  $[\theta_{3min}, 0]$ , and  $[\theta_{4min}, \theta_{4max}]$  are the joint limits of the waist, shoulder, elbow, and wrist, respectively. The angles  $\theta_1$  and  $\theta_2$  consider the positive direction of the horizontal x-axis as a reference, and  $\theta_3$  takes the extension of the upper arm as a reference. During the picking process, the end-effector is always maintained horizontally. We set the counterclockwise rotation as the positive direction of the rotation angles.

## 2.2. Kinematics model of the articulated manipulator

### 2.2.1. Forward kinematics

The forward kinematics modeling of the articulated manipulator was driven using the Denavit Hartenberg method [23], [24]. This method is commonly used to calculate the forward kinematics equation of the multijoint manipulator. There are three main steps in the Denavit Hartenberg method. The first step is to assign the coordinate frame to each joint in the kinematic diagram of the manipulator according to the frame rules of the Denavit-Hartenberg convention [25], as shown in Figure 2.

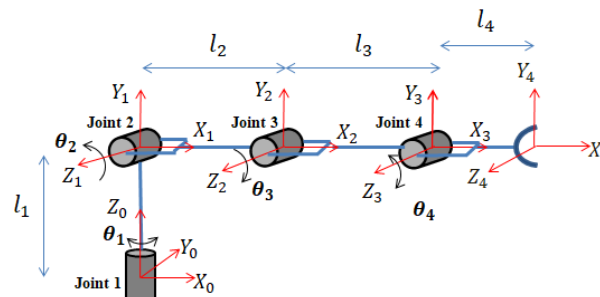


Figure 2. Kinematic diagram of the manipulator

In the second step, we fill in the Denavit-Hartenberg parameters in Table 1 using the kinematic diagram of the manipulator. The four parameters are  $\theta_n$ ,  $d_n$ ,  $r_n$ , and  $\alpha_n$ .  $\theta_n$  is the angle between  $X_{n-1}$  and  $X_n$  measured around  $Z_{n-1}$ .  $\alpha_n$  is the angle between  $Z_{n-1}$  and  $Z_n$  measured around  $X_n$ .  $r_n$  is the distance along the  $X_n$  direction from the origin of frame  $n-1$  to the origin of frame  $n$ .  $d_n$  is the distance along the  $Z_{n-1}$  direction from the origin of frame  $n-1$  to the origin of frame  $n$ .

Table 1. Denavit Hartenberg parameters of the manipulator

Joint n	$\theta_n$ (°)	$\alpha_n$ (°)	$r_n$ (meter)	$d_n$ (meter)
1	$\theta_1$	90°	0	$l_1$
2	$\theta_2$	0	$l_2$	0
3	$\theta_3$	0	$l_3$	0
4	$\theta_4$	0	$l_4$	0

The third step of the Denavit Hartenberg method is to insert the four parameters of Table 1 into the homogenous transformation matrix from frame n-1 to frame n,

$$H_n^{n-1} = \begin{bmatrix} \cos \theta_n & -\sin \theta_n \cos \alpha_n & \sin \theta_n \sin \alpha_n & r_n \cos \theta_n \\ \sin \theta_n & \cos \theta_n \cos \alpha_n & -\cos \theta_n \sin \alpha_n & r_n \sin \theta_n \\ 0 & \sin \alpha_n & \cos \alpha_n & d_n \\ 0 & 0 & 0 & 1 \end{bmatrix} = \begin{bmatrix} R_n^{n-1} & T_n^{n-1} \\ 0 & 1 \end{bmatrix} \quad (1)$$

Where  $T_n^{n-1}$  represents the displacement vector from frame n-1 to frame n, and  $R_n^{n-1}$  is the rotation matrix from frame n-1 to frame n. The homogenous transformation matrix from frame 0 to frame 4 is expressed as (2):

$$H_4^0 = H_1^0 \times H_2^1 \times H_3^2 \times H_4^3 \quad (2)$$

From the displacement vector  $T_4^0$  of the matrix  $H_4^0$ , we can determine the position of the end-effector relative to the base as (3):

$$T_4^0 = \begin{bmatrix} x_4 \\ y_4 \\ z_4 \end{bmatrix} = \begin{bmatrix} (l_2 \times \cos(\theta_2) + l_3 \times \cos(\theta_2 + \theta_3) + l_4 \times \cos(\theta_2 + \theta_3 + \theta_4)) \times \cos(\theta_1) \\ (l_2 \times \cos(\theta_2) + l_3 \times \cos(\theta_2 + \theta_3) + l_4 \times \cos(\theta_2 + \theta_3 + \theta_4)) \times \sin(\theta_1) \\ l_1 + l_2 \times \sin(\theta_2) + l_3 \times \sin(\theta_2 + \theta_3) + l_4 \times \sin(\theta_2 + \theta_3 + \theta_4) \end{bmatrix} \quad (3)$$

### 2.2.2. Inverse kinematics

We use the geometric method to solve the manipulator's inverse kinematics [26], [27]. The joint angular positions that correspond to the target end-effector position ( $x_4$ ,  $y_4$ ,  $z_4$ ) were determined by considering that the end-effector keeps a horizontal orientation. By employing this methodology, the expressions of joint angular positions are given,

$$\begin{cases} \theta_1 = \tan^{-1} \frac{y_4}{x_4} \\ \theta_2 = \tan^{-1} \frac{z_4 - l_1}{\sqrt{x_4^2 + y_4^2} - l_4} + \cos^{-1} \left( \frac{l_2^2 + (\sqrt{x_4^2 + y_4^2} - l_4)^2 + (z_4 - l_1)^2 - l_3^2}{2 l_2 \sqrt{(\sqrt{x_4^2 + y_4^2} - l_4)^2 + (z_4 - l_1)^2}} \right) \\ \theta_3 = -\cos^{-1} \left( \frac{-l_2^2 - l_3^2 + (\sqrt{x_4^2 + y_4^2} - l_4)^2 + (z_4 - l_1)^2}{2 l_2 l_3} \right) \\ \theta_4 = -\theta_2 - \theta_3 \end{cases} \quad (4)$$

## 2.3. Workspace optimization

### 2.3.1. Identify the manipulator's harvesting zone

Identifying the spatial requirements for each step of the fruit-picking cycle is crucial for determining the reachability requirements of the manipulator. This ensures that the manipulator can access the distribution space of the strawberries effectively and perform the fruit-picking cycle efficiently. Each picking cycle of the arm robot consists of a sequence of steps: the displacement of the end effector from the initial position towards the ripe fruit. After detaching the strawberry from the plant, the end-effector steps back horizontally by 100 mm from the plant to prevent collision while transporting the harvested strawberries to the container. Once the fruit is released into the container, the end-effector returns to its initial position to complete the harvesting cycle.

The distribution of ripe strawberries in a plant is defined as follows: the height range (on the z-axis) is 850–1100 mm, with a width of 200 mm (on the x-axis) and a length of approximately 350 mm (on the y-axis), as shown in Figure 1. Based on the growth characteristics of the fruits, we consider that the distribution space of the strawberries has the shape of a cuboid, with length (L), width (W), and height (H) equal to 350 mm, 200 mm, and 250 mm, respectively. The dimensions of the cuboid are adjusted to accommodate the spatial requirements of the fruit-picking cycle, which include approaching the target

strawberry from the initial picking position and stepping back the end-effector after detaching the harvest. The end-effector's initial picking position is at least 100 mm away from the planting row and facing the opposite direction of the row. This involves expanding the cuboid to new dimensions  $L \times W' \times H$ , with  $W'=300$  mm, to ensure it encloses the necessary volume for the manipulator's movements.

### 2.3.2. Analyzing the enclosure of harvesting space by manipulator workspace

The problem of enclosing the cuboid with dimensions  $L \times W' \times H$  within the manipulator's workspace can be simplified by addressing the enclosure of a rectangle with dimensions  $W'' \times H$  in the vertical plane ( $xoz$ ), as shown in Figure 3(a), and the rotation of the waist joint around the  $z$ -axis with a corresponding angular range  $\Delta\theta_1$ , as depicted in Figure 3(b). This allows the manipulator to cover the entire cuboid effectively [18], [28].  $\Delta\theta_1$  and  $W''$  are given as (5):

$$\begin{cases} \Delta\theta_1 \geq 2 \times \tan^{-1}\left(\frac{L/2}{r_1}\right) \\ W'' = r_2 - r_1 \end{cases} \quad (5)$$

The  $r_1$  and  $r_2$  represent the arc radius of the actual manipulator workspace limit on the  $xy$ -plane, as represented in Figure 3(b);  $r_1$  is the distance between origin  $O$  and the left periphery of the cuboid,  $r_1=260$  mm. Completing the calculation, we obtain  $\Delta\theta_1 \geq 68^\circ$  and  $W''=327$  mm.

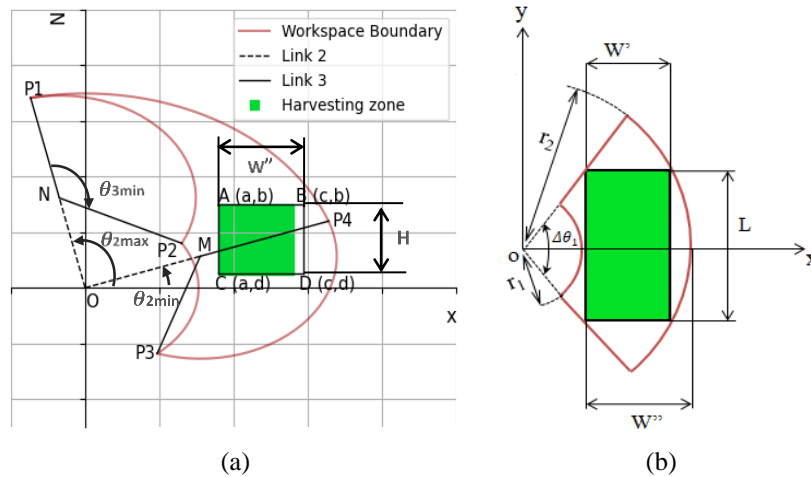


Figure 3. Target picking area: (a) view in the  $xz$  plane and (b) view in the  $xy$  plane

The objective of this study is to determine the minimal workspace dimensions of the manipulator while ensuring it covers the entire picking space. The manipulator's working space size depends on the length of the links and the angle range of the joints. To proceed with the optimization design process, in this part we simplified dealing with the target harvesting zone in order to facilitate the construction of the mathematical model.

### 2.3.3. Mathematical model of the optimization problem

The objective is to search for the minimum area of the actual workspace  $P1P2P3P4$  that contains the rectangle  $ABCD$  by optimizing the structural parameters of the manipulator. First, we have to determine the area for  $P1P2P3P4$  ( $S_{P1P2P3P4}$ ). From Figure 3(a), the formula of  $S_{P1P2P3P4}$  is given,

$$\begin{aligned} S_{P1P2P3P4} &= \frac{(\alpha_{P1} - \alpha_{P4}) \times r_{OP1}^2 - (\alpha_{P2} - \alpha_{P3}) \times r_{OP3}^2}{2} \\ &= (\theta_{2max} - \theta_{2min}) \times l_2 \times l_3 \times (1 - \cos(\theta_{3min})) \end{aligned} \quad (6)$$

Where  $\alpha_i$  is the angle between the positive direction of the  $x$ -axis and the vector  $\vec{OI}$ .

The optimization problem has been presented by a mathematical model, defining the kinematic parameters as optimization variables,  $S_{P1P2P3P4}$  as the objective function that should be optimized, and the

enclosure of the rectangle ABCD within the manipulator's workspace boundaries as constraint functions. This presentation of the problem will facilitate achieving an optimal solution, and it is given by;

Optimization variables: the area  $S_{P_1P_2P_3P_4}$  is a function of  $l_2$ ,  $l_3$ ,  $\theta_{2min}$ ,  $\theta_{2max}$ , and  $\theta_{3min}$ . The length of the first link primarily influences the vertical position of the workspace. The length of the last link primarily influences the horizontal position of the workspace. These two parameters affect the length of other links and the angular range of the joints. The length of the first and last links may indirectly influence the area of the manipulator's workspace. But their impact would likely be minimal compared to other structural parameters. So, the designed kinematic parameters of the manipulator that need to be optimized are five,

$$X = [x_1, x_2, x_3, x_4, x_5] = [l_2, l_3, \theta_{2min}, \theta_{2max}, \theta_{3min}] \quad (7)$$

The objective function: the objective function is expressed by,

$$\min f(x) = \min (S_{P_1P_2P_3P_4}) \quad (8)$$

The constraints: the rectangle ABCD must be enveloped by the four arcs  $\widehat{P_1P_4}$ ,  $\widehat{P_4P_3}$ ,  $\widehat{P_1P_2}$ , and  $\widehat{P_2P_3}$ . According to the specific functional and operational requirements of strawberry harvesting,  $l_4$  is equal to 150 mm. As the height range of strawberry distribution is 850–1100 mm and the height of the platform on which the robotic manipulator was placed was around 500 mm, the length of the first link was set at 300 mm so that the robotic manipulator could face the picking area. The shoulder joint center was taken as the coordinate origin; combined with Figures 1 and 3(a), the x and z coordinates of the four points in the rectangular ABCD, A (a,b), B (c,b), C (a,d), and D (c,d), are equal to a=110 mm, b=300 mm, c=437 mm, and d=50 mm. There are four constraints to be respected, each associated with an arc. We add the fifth constraint, corresponding to the length of the upper arm being equal to the length of the lower arm, to obtain a compact and flexible manipulator structure [18].

Constraint (1): in the arc  $\widehat{P_1P_4}$  at  $z=b$ ,  $\sqrt{b^2 + c^2} \leq r_{OP_1}$ .

Constraint (2): in the arc  $\widehat{P_4P_3}$  at  $z=d$ ,  $x_M + l_3 \times \cos(\beta) \geq c$ , where  $\beta = \tan^{-1}\left(\frac{l_2 \times \sin(\theta_{2min}) - d}{c - l_2 \times \cos(\theta_{2min})}\right)$

Constraint (3): in the arc  $\widehat{P_1P_2}$  at  $z=z_N$ ,  $x_N + l_3 \leq a$ .

Constraint (4): in the arc  $\widehat{P_2P_3}$  at  $z=d$ ,  $r_{OP_2} \leq \sqrt{a^2 + d^2}$

Constraint (5):  $l_2=l_3$ .

### 2.3.4. GlobalSearch algorithm

The genetic and PSO algorithms are known for their robustness in finding global minima, but they may not always guarantee finding the global optimum. The effectiveness of each algorithm may vary depending on the specific characteristics of the optimization problem. It is recommended to analyze the nature of the optimization problem before selecting any optimization algorithm.

We have a smooth problem with smooth objective and constraint functions. The problem's objective function is nonlinear, multivariable, and non-convex. The GlobalSearch algorithm was adopted because it is specifically designed to handle this type of problem (smooth, nonlinear, and non-convex optimization problems with multiple constraints) [29]. The GlobalSearch solver from MATLAB's global optimization Toolbox was used. It locates the global minimum solution by using a precise and fastest local solver, fmincon, with the sequential quadratic programming algorithm (SQP) [29]. There are a moderate number of decision variables and constraints in the optimization problem. The SQP algorithm performs well for medium-sized problems. The GlobalSearch starts by running fmincon from the provided starting point,  $X_0$ . In stages 1 and 2, the solver generates a random set of starting points. After that, it filters them before running the fmincon solver. Table 2 sets out the simulation parameters. Figure 4 presents a summary diagram of the GlobalSearch solver steps. For a more detailed description of the GlobalSearch algorithm, see [29], [30].

Table 2. The values of the simulation parameters

Parameters	Value
Algorithm	SQP
Number of trial points	2000
Number of trial points in stage 1	200
The maximum time that GlobalSearch runs	Infinity
$X_0$	[0.4 m, 0.4 m, 0.35 rad, 1.2 rad, -1.92 rad]

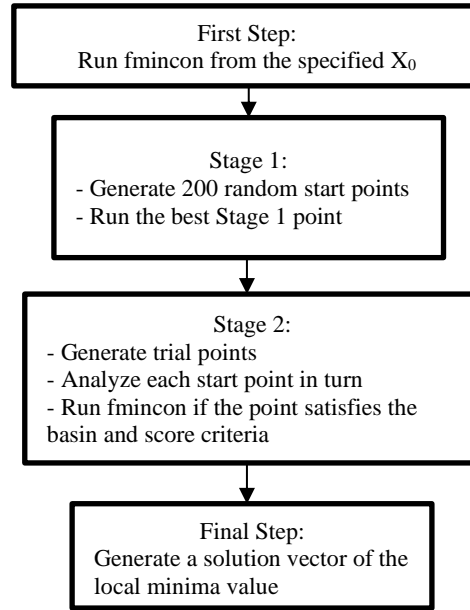


Figure 4. Flowchart of the GlobalSearch solver steps

## 2.4. Trajectory planning

The motion of the manipulator during each step of fruit picking is conducted in joint space. A trigonometric S-curve trajectory planning with the modified sine jerk model [31] is adopted to generate the joint path from the start pose to the desired pose. This trajectory model compromises between motion smoothness, speed, and computational complexity. It is able to generate faster trajectories while respecting joint limits; its execution time is up to 12% and 7% shorter than that of the trigonometric S-curve trajectory approach with a three-phase sine jerk motion profile and the 4–5–6–7 polynomial method, respectively [31]. This trajectory-planning approach maintains smooth motion, leading to improved tracking accuracy, which is important for handling fragile strawberries in confined environments. The motion profile consists of fifteen segments that present the equational variation of jerk. The modified sine jerk profile is defined as (9):

$$j(t) = \begin{cases} J_{peak} \sin\left(\frac{\pi}{2T_1} \tau_i\right), & t_0 \leq t < t_1, t_{12} \leq t < t_{13} \\ J_{peak}, & t_1 \leq t < t_2, t_{13} \leq t < t_{14} \\ J_{peak} \sin\left(\frac{\pi}{2}\left(1 + \frac{\tau_i}{T_1}\right)\right), & t_2 \leq t < t_3, t_{14} \leq t \leq t_{15} \\ 0, & t_3 \leq t < t_4, t_7 \leq t < t_8, t_{11} \leq t < t_{12} \\ -J_{peak} \sin\left(\frac{\pi}{2T_1} \tau_i\right), & t_4 \leq t < t_5, t_8 \leq t < t_9 \\ -J_{peak}, & t_5 \leq t < t_6, t_9 \leq t < t_{10} \\ -J_{peak} \sin\left(\frac{\pi}{2}\left(1 + \frac{\tau_i}{T_1}\right)\right), & t_6 \leq t < t_7, t_{10} \leq t < t_{11} \end{cases} \quad (9)$$

$J_{peak}$  is the peak value of jerk. For every segment,  $t_i$  ( $i=0, 1, \dots, 15$ ) is the time boundary. The interval of time of each segment is  $T_i=t_i-t_{i-1}$  ( $i=1, \dots, 15$ ), and  $\tau_i=t-t_{i-1}$  is the time relative to the commencement of the interval  $[t_{i-1}, t_i]$  ( $i=1, \dots, 15$ ). The acceleration, velocity, and displacement functions of the trajectory are given by integrating the jerk function,

$$\begin{cases} a(t) = a(t_i) + \int_{t_i}^t j(t) dt \\ v(t) = v(t_i) + \int_{t_i}^t a(t) dt \\ d(t) = d(t_i) + \int_{t_i}^t v(t) dt \end{cases} \quad (10)$$

### 3. RESULTS AND DISCUSSION

#### 3.1. The workspace optimization

The proposed optimization process was conducted on a 4-DoF articulated manipulator. The GlobalSearch solver successfully determines the optimal structural parameters of the manipulator, minimizing the area of the workspace. The results of the optimization are summarized in Table 3. To accommodate the step of transferring fruit to the container placed on the mobile platform, the base of the manipulator must be rotated 90°. This will guarantee that the manipulator successfully completes every step of the fruit-picking cycle. Additionally, the manipulator will harvest the fruits grown on both sides of the robot by rotating the waist joint 180°. These adjustments expand the angle range of  $\theta_1$  from  $[-34^\circ, 34^\circ]$  to  $[-34^\circ, 214^\circ]$ . Table 4 presents the values of all structural parameters.

Table 3. Optimization results

Parameters	Values
$X=[l_2, l_3, \theta_{2min}, \theta_{2max}, \theta_{3min}]$	$[0.265 \text{ m}, 0.265 \text{ m}, 0.6 \text{ rad}, 2.2 \text{ rad}, -2.7 \text{ rad}]$
The workspace's area $S_{P1P2P3P4}$	$0.2125 \text{ m}^2$

Table 4. Structural parameters of the harvesting manipulator

i	Link i length (mm)	Range of joint angle i
1	300	$[-34^\circ, 214^\circ]$
2	265	$[34.4^\circ, 126^\circ]$
3	265	$[-155^\circ, 0^\circ]$
4	150	$[-126^\circ, 121^\circ]$

We simulate the workspace of the robot using the forward kinematics equation to ensure coverage of the picking zone. Figure 5 presents the simulation of the manipulator workspace. The cuboid in Figure 5(a) represents the harvesting space, and the rectangle in Figure 5(b) represents its projection in the xz-plane. From the simulation results, the optimal design of the manipulator can effectively cover the designated harvesting area. The robot will generate the same workspace in the left and right plant rows.

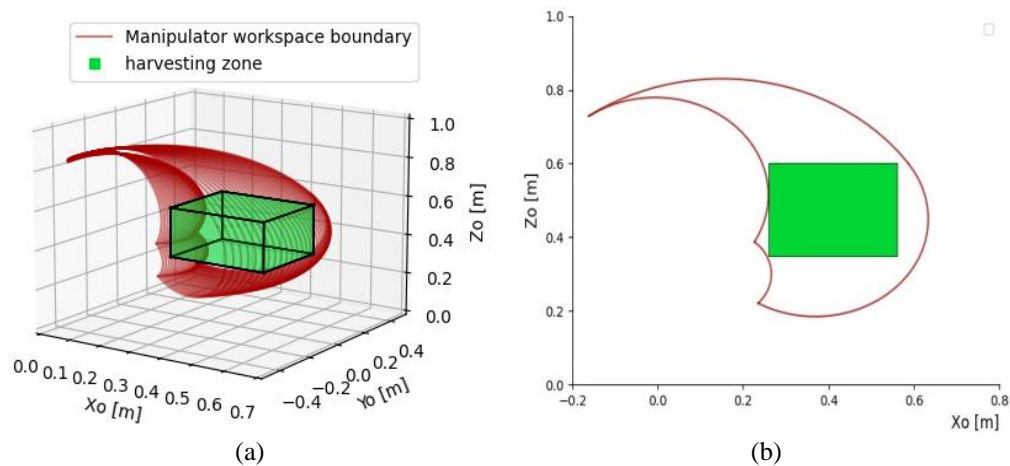


Figure 5. The manipulator workspace boundary simulation results in; (a) the workspace in 3 dimensions and (b) the workspace projection in the xz-plane

This study focuses on the spatial requirements of the fruit-picking cycle, aiming to understand the spatial dynamics beyond the fruit distribution area. Previous research primarily focused on fruit distribution areas but overlooked other critical stages of the fruit-picking process [13], [15], [17], [28]. Even if we address the spatial needs of several steps of harvesting at once, the workspace model method facilitates the optimization of the manipulator structure parameters. This optimization not only minimizes unnecessary movements but also reduces the risk of collisions and damage to both the manipulator and surrounding crops, and the manipulator movements can be better optimized.



### 3.2. Trajectory planning

We simulate a path in joint space to demonstrate the effectiveness of this trajectory planning model. Specifically, we guide the manipulator's gripper from the initial position  $P_0$  ( $x_4=0.227$  m,  $y_4=0$  m,  $z_4=0.39$  m) to the target fruit position  $P_1$  ( $x_4=0.56$  m,  $y_4=0.175$  m,  $z_4=0.589$  m). The joint angular positions for points  $P_1$  and  $P_2$  are calculated using inverse kinematics and are given in Table 5. The joint motion profiles were obtained by simulation with MATLAB software. Figures 6(a) to (d) illustrates the displacement, velocity, acceleration, and jerk curves of the four joints. The generated trajectory ensures higher levels of continuity up to jerk during the whole motion. Thus, the arm robot tracks the generated trajectory without any abrupt change. It is beneficial to suppress the vibrations of the robot's movement and enhance position accuracy.

Table 5. Angular joint position for target points

Joint	1	2	3	4
Position $P_0$ (rad)	0	2.2	-2.7	0.3
Position $P_1$ (rad)	0.3	0.73	-0.3	-0.43

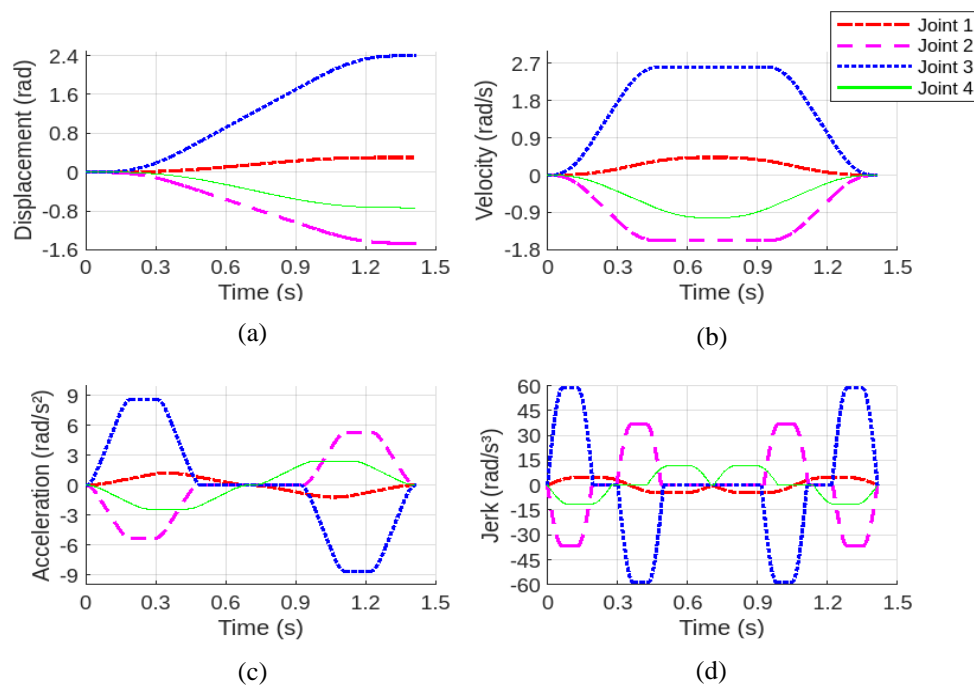


Figure 6. The resulting motion profiles of the four joints obtained by modified sine jerk trajectory planning are: (a) displacement, (b) velocity, (c) acceleration, and (d) jerk

We calculate the time trajectory for four generated paths from the initial position to the target fruit position; the results are presented in Table 6. By adopting the modified sine jerk model in the optimal design of the manipulator, the average time to approach the fruit from the initial position is 1.1 s. The time required to approach the target fruit in other studies is about 1.5 s [7], [32]. The execution time is reduced by approximately 27%. This approach can reduce the execution time of each step of the picking cycle, which reduces harvesting time and improves productivity.

Table 6. Fruit approaching time

Fruit position (m)			Execution time (s)
$X_4$	$Y_4$	$Z_4$	
0.4	0.17	0.5	0.95691
0.36	0.1	0.56	0.97765
0.56	0	0.35	1.3743

#### 4. CONCLUSION

This study addressed the issue of optimizing both the structural parameters of the robotic manipulator and its trajectory design. We propose an approach for optimizing the manipulator's structural parameters to minimize its workspace, which combines the workspace model method, mathematical modeling, and the GlobalSearch algorithm. By addressing the spatial requirements of different stages of the fruit-picking cycle in the optimization process, we ensure that the manipulator's workspace can effectively cover the picking area while occupying the smallest possible physical space. This guarantees better performance, adaptability, and safety in harvesting operations. After that, we explore the optimal trajectory planning method, which compromises between motion smoothness, speed, and computational complexity by adopting a modified sine jerk model. The effectiveness of this method was demonstrated through the simulation of the joint trajectories to drive the end effector from the initial position to the position of the strawberry. This approach yields execution times up to 27% shorter than previous studies. Even though this optimization approach was initially developed for a 4-DoF articulated robot, its fundamental techniques are sufficiently general to be used with a wider variety of robotic systems with different joint configurations.

Our present research has primarily focused on kinematic aspects in the design and trajectory planning of manipulator systems; incorporating dynamics considerations can significantly improve the robot system's capabilities and performance. In future work, it is important to address dynamics-related gaps in our study findings. This involves developing dynamic models and designing control algorithms that account for dynamic effects. By combining dynamic issues, we can produce more effective solutions that are more adapted to the requirements of the actual agricultural environment.

#### ACKNOWLEDGEMENTS

This research was supported in part by the National Center for Scientific and Technical Research (CNRST) in Morocco through its Research Scholarships Grants program, under Grant Agreement number 29UAE2021.




#### REFERENCES

- [1] S. Fountas, N. Mylonas, I. Malounas, E. Rodias, C. H. Santos, and E. Pekkeriet, "Agricultural Robotics for Field Operations," *Sensors*, vol. 20, no. 9, p. 2672, May 2020, doi: 10.3390/s20092672.
- [2] J. Jun, J. Kim, J. Seol, J. Kim, and H. I. Son, "Towards an Efficient Tomato Harvesting Robot: 3D Perception, Manipulation, and End-Effector," *IEEE Access*, vol. 9, pp. 17631–17640, 2021, doi: 10.1109/ACCESS.2021.3052240.
- [3] Y. Yu, K. Zhang, H. Liu, L. Yang, and D. Zhang, "Real-Time Visual Localization of the Picking Points for a Ridge-Planting Strawberry Harvesting Robot," *IEEE Access*, vol. 8, pp. 116556–116568, 2020, doi: 10.1109/ACCESS.2020.3003034.
- [4] W. Mao, H. Liu, W. Hao, F. Yang, and Z. Liu, "Development of a Combined Orchard Harvesting Robot Navigation System," *Remote Sensing*, vol. 14, no. 3, p. 675, Jan. 2022, doi: 10.3390/rs14030675.
- [5] S. Wang *et al.*, "Design, development and evaluation of latex harvesting robot based on flexible Toggle," *Robotics and Autonomous Systems*, vol. 147, p. 103906, Jan. 2022, doi: 10.1016/j.robot.2021.103906.
- [6] Y. Ma, W. Zhang, W. S. Qureshi, C. Gao, C. Zhang, and W. Li, "Autonomous navigation for a wolfberry picking robot using visual cues and fuzzy control," *Information Processing in Agriculture*, vol. 8, no. 1, pp. 15–26, Mar. 2021, doi: 10.1016/j.inpa.2020.04.005.
- [7] G. Hu *et al.*, "Simplified 4-DOF manipulator for rapid robotic apple harvesting," *Computers and Electronics in Agriculture*, vol. 199, p. 107177, Aug. 2022, doi: 10.1016/j.compag.2022.107177.
- [8] Y. Xiong, C. Peng, L. Grimstad, P. J. From, and V. Isler, "Development and field evaluation of a strawberry harvesting robot with a cable-driven gripper," *Computers and Electronics in Agriculture*, vol. 157, pp. 392–402, Feb. 2019, doi: 10.1016/j.compag.2019.01.009.
- [9] Y. Xiong, Y. Ge, L. Grimstad, and P. J. From, "An autonomous strawberry-harvesting robot: Design, development, integration, and field evaluation," *Journal of Field Robotics*, vol. 37, no. 2, pp. 202–224, Mar. 2020, doi: 10.1002/rob.21889.
- [10] A. Buerkle *et al.*, "Towards industrial robots as a service (IRaaS): Flexibility, usability, safety and business models," *Robotics and Computer-Integrated Manufacturing*, vol. 81, p. 102484, Jun. 2023, doi: 10.1016/j.rcim.2022.102484.
- [11] A. Perzylo *et al.*, "SMERobotics: Smart Robots for Flexible Manufacturing," in *IEEE Robotics & Automation Magazine*, vol. 26, no. 1, pp. 78–90, March 2019, doi: 10.1109/MRA.2018.2879747.
- [12] Y. Jing, L. Jin, X. Shi, D. Zhao, and M. Hu, "Dimensional Optimization for Minimally Invasive Surgery Robot Based on Double Space and Kinematic Accuracy Reliability Index," *Journal of Engineering and Science in Medical Diagnostics and Therapy*, vol. 3, no. 2, Feb. 2020, doi: 10.1115/1.4046382.
- [13] Z. Xiong *et al.*, "Dual-Manipulator Optimal Design for Apple Robotic Harvesting," *Agronomy*, vol. 12, no. 12, p. 3128, Dec. 2022, doi: 10.3390/agronomy12123128.
- [14] J. Sun, Z. Yan, and Z. Du, "Optimal design of a novel remote center-of-motion mechanism for minimally invasive surgical robot," *IOP Conference Series: Earth and Environmental Science*, vol. 69, no. 1, Jun. 2017, doi: 10.1088/1755-1315/69/1/012097.
- [15] S. Zhang, T. Yuan, D. Wang, J. Zhang, and W. Li, "Structure Optimization and Path Planning of Tomato Picking Manipulator," in *2016 9th International Symposium on Computational Intelligence and Design (ISCID)*, Hangzhou: IEEE, Dec. 2016, pp. 356–360, doi: 10.1109/ISCID.2016.2091.
- [16] Y. Zhu, B. Jin, W. Li, and S. Li, "Optimal design of hexapodwalking robot leg structure based on energy consumption and workspace," *Transactions- Canadian Society for Mechanical Engineering*, vol. 38, no. 4, pp. 305–317, Sep. 2014, doi: 10.1139/tcsme-2014-0022.




- [17] Q. Zhao, L. Li, Z. Wu, X. Guo, and J. Li, "Optimal Design and Experiment of Manipulator for Camellia Pollen Picking," *Applied Sciences*, vol. 12, no. 16, p. 8011, Aug. 2022, doi: 10.3390/app12168011.
- [18] J. Wu, Y. Zhang, S. Zhang, H. Wang, L. Liu, and Y. Shi, "Simulation Design of a Tomato Picking Manipulator," *Tehnicki Vjesnik*, vol. 28, no. 4, pp. 1253–1261, Jul. 2021, doi: 10.17559/TV-20210323084618.
- [19] X. Cao *et al.*, "A Multi-Objective Particle Swarm Optimization for Trajectory Planning of Fruit Picking Manipulator," *Agronomy*, vol. 11, no. 11, p. 2286, Nov. 2021, doi: 10.3390/agronomy11112286.
- [20] X. Hu, H. Yu, S. Lv, and J. Wu, "Design and experiment of a new citrus harvesting robot," in *2021 International Conference on Control Science and Electric Power Systems (CSEPS)*, May 2021, pp. 179–183, doi: 10.1109/CSEPS53726.2021.00043.
- [21] H. Z. Ting, M. H. M. Zaman, M. F. Ibrahim, and A. M. Moubark, "Kinematic Analysis for Trajectory Planning of Open-Source 4-DoF Robot Arm," *International Journal of Advanced Computer Science and Applications (IJACSA)*, vol. 12, no. 6, 2021, doi: 10.14569/IJACSA.2021.0120690.
- [22] F. Molaei and S. Ghatreh Samani, "Kinematic-Based Multi-Objective Design Optimization of a Grapevine Pruning Robotic Manipulator," *AgriEngineering*, vol. 4, no. 3, pp. 606–625, Jul. 2022, doi: 10.3390/agriengineering4030040.
- [23] J. Denavit and R. S. Hartenberg, "A Kinematic Notation for Lower-Pair Mechanisms Based on Matrices," *Journal of Applied Mechanics*, vol. 22, no. 2, pp. 215–221, Jun. 1955, doi: 10.1115/1.4011045.
- [24] G. Močnik, Z. Kačič, R. Šafarič, and I. Mlakar, "Capturing Conversational Gestures for Embodied Conversational Agents Using an Optimized Kaneda–Lucas–Tomas Tracker and Denavit–Hartenberg-Based Kinematic Model," *Sensors*, vol. 22, no. 21, Jan. 2022, doi: 10.3390/s22218318.
- [25] F. Ding and C. Liu, "Applying coordinate fixed Denavit–Hartenberg method to solve the workspace of drilling robot arm," *International Journal of Advanced Robotic Systems*, vol. 15, no. 4, Jul. 2018, doi: 10.1177/1729881418793283.
- [26] M. W. Spong, S. Hutchinson, and M. Vidyasagar, "Inverse Kinematics," in *Robot Dynamics and Control*, 2nd ed., Wiley New York, 2004, pp. 79–89.
- [27] Z. Mohamed and G. Capi, "Development of a New Mobile Humanoid Robot for Assisting Elderly People," *Procedia Engineering*, vol. 41, pp. 345–351, Dec. 2012, doi: 10.1016/j.proeng.2012.07.183.
- [28] Y. Wang, Q. Yang, G. Bao, Y. Xun, and L. Zhang, "Optimization Design and Experiment of Fruit and Vegetable Picking Manipulator," *Transactions of the Chinese Society for Agricultural Machinery*, vol. 42, pp. 191–195, 2011.
- [29] The MathWorks, Inc, "Using GlobalSearch and MultiStart," in *MATLAB Global Optimization Toolbox User's Guide*, R2020a ed., 2020.
- [30] Z. Ugray, L. Lasdon, J. Plummer, F. Glover, J. Kelly, and R. Marti, "Scatter Search and Local NLP Solvers: A Multistart Framework for Global Optimization," *INFORMS Journal on Computing*, vol. 19, no. 3, pp. 328–340, Aug. 2007, doi: 10.1287/ijoc.1060.0175.
- [31] Y. Fang, J. Qi, J. Hu, W. Wang, and Y. Peng, "An approach for jerk-continuous trajectory generation of robotic manipulators with kinematical constraints," *Mechanism and Machine Theory*, vol. 153, p. 103957, Nov. 2020, doi: 10.1016/j.mechmachtheory.2020.103957.
- [32] Q. Feng *et al.*, "Design and test of robotic harvesting system for cherry tomato," *International Journal of Agricultural and Biological Engineering*, vol. 11, no. 1, pp. 96–100, 2018, doi: 10.25165/j.ijabe.20181101.2853.

## BIOGRAPHIES OF AUTHORS






**Inas Saoud**    received the Engineer degree in mechatronics engineering from the National School of Applied Sciences (ENSA), Abdelmalek Essaadi University, Tetuan, Morocco, in 2020. She is currently pursuing a Ph.D. in robotics at the National School of Applied Sciences in Tangier, Morocco. Her research focuses on agricultural robots, modeling and design, robotic device development, control, and optimization. She can be contacted at email: inas.saoud@etu.uae.ac.ma.






**Hatim Idriss Jaafari**    obtained a master's degree in cybersecurity and cybercriminality from Abdelmalek Essaadi University, ENSA Tangier, Morocco, in 2021. He is currently a Ph.D. student in the domain of secure communications in robotic operating systems and a member of the Mathematics and Intelligent Systems Research Team. His research focuses on securing communication channels, safeguarding data through encryption methods, and exploring the potential of blockchain technology to enhance security in various domains. He can be contacted at email: hatimidriss.jaafari@etu.uae.ac.ma.






**Asaad Chahboun**    is a highly qualified professional with an extensive educational background in telecommunications. He holds an M.S. and a Ph.D. degree in telecommunications from Abdelmalek Essaadi University and an engineering degree from the Central School of Arts and Businesses in Brussels, Belgium. He has diverse work experience, which includes working as a maintenance-responsible engineer of radiology and medical imaging materials in Rabat, Morocco. Currently, he is a member of the Mathematics and Intelligent Systems research team in the Department of Information Systems and Communication at the National School of Applied Sciences in Tangier, Morocco, at the University of Abdelmalek Essaâdi. As a researcher, his focus is on several areas of interest, including wireless sensor networks, routing in ad hoc networks, the internet of things, network security, remote sensing, the development of remote sensing methods for land cover dynamic monitoring, and grid computing. He can be contacted at email: achahboun@uae.ac.ma.






**Naoufal Raissouni**    received M.S. and Ph.D. degrees in physics (remote sensing, earth observation, and geoscience) at the Global Change Unit at the University of Valencia, Spain, in collaboration with Louis Pasteur University, 212 Strasbourg, France, and the Centre National de la Recherche Scientifique, France. He is a professor and researcher in physics and remote sensing at the National Engineering School for Applied Sciences of Tetuan at the University of Abdelmalek Essaadi (UAE), Morocco. He heads the Remote Sensing and Geographic Information System Laboratory in the UAE, and he is president of the Remote Sensing and GIS Association in Morocco. He has been heading the Innovation and Telecoms Engineering research group and the RSAID Laboratory. His research interests include the retrieval of emissivity, atmospheric water vapor, and sea/land surface temperature from satellite images; wireless sensor networks; infrared radiometry; and in situ measurements. He can be contacted at email: nraissouni@uae.ma.



**Nizar Ben Achhab**    received a Ph.D. degree in telecommunications and informatics in 2011 and an M.S. degree in bioinformatics in 2004 from the University of Abdelmalek Essaadi (UAE), Tetuan, Morocco. Currently, he is a member of the Mathematics and Intelligent Systems Research Team. His current work includes remote sensing multitemporal and spatiotemporal studies of thermal infrared satellite imagery of the earth's surface, in-situ LST measurements, and the development of remote sensing methods for land cover dynamic monitoring. It also includes grid computing, multithreading, GPGPU, and hardware and software methods for time computing optimizations. He can be contacted at email: nbenachhab@uae.ac.ma.



**Abdelilah Azyat**    received a Ph.D. degree in telecommunications and informatics in 2011 and an M.S. degree in bioinformatics in 2004 from the University of Abdelmalek Essaadi (UAE), Tetuan, Morocco. Currently, he is a member of the Mathematics and Intelligent Systems Research Team. His research interests include remote sensing, spatiotemporal studies of thermal infrared satellite imagery of the earth's surface, GIS, and mobile GIS. He can be contacted at email: aazyat@uae.ac.ma.